TYPE Original Research
PUBLISHED 10 November 2025
DOI 10.3389/feart.2025.1687382



OPEN ACCESS

EDITED BY
Tao Hu,
China University of Petroleum, Beijing, China

REVIEWED BY
Zhikai Liang,
China University of Petroleum, China
Chengwu Xu,
Northeast Petroleum University, China

*CORRESPONDENCE

Xin He,

is xinlwfbyx_2025@163.com

Lei Zhang,
is zhlkeyan@163.com

RECEIVED 17 August 2025 REVISED 27 September 2025 ACCEPTED 09 October 2025 PUBLISHED 10 November 2025

CITATION

He X, Wang R, Zhang X, Zhang L, Gao R, Liu R and Lei W (2025) Multi-lithofacies pore-structure oil-bearing differences and shale oil enrichment model of the Es4 shale in the western sag of Liaohe, Bohai Bay Basin. Front. Earth Sci. 13:1687382. doi: 10.3389/feart.2025.1687382

COPYRIGHT

© 2025 He, Wang, Zhang, Zhang, Gao, Liu and Lei. This is an open-access article distributed under the terms of the Creative Commons Attribution License (CC BY). The use, distribution or reproduction in other forums is permitted, provided the original author(s) and the copyright owner(s) are credited and that the original publication in this journal is cited, in accordance with accepted academic practice. No use, distribution or reproduction is permitted which does not comply with these terms.

Multi-lithofacies pore-structure oil-bearing differences and shale oil enrichment model of the Es4 shale in the western sag of Liaohe, Bohai Bay Basin

Xin He^{1*}, Ruifei Wang¹, Xuejuan Zhang², Lei Zhang^{2*}, Rongjin Gao³, Ruhao Liu² and Wenwen Lei³

¹College of Petroleum Engineering, Xi'an Shiyou University, Xi'an, China, ²School of Petroleum Engineering, Chongqing University of Science and Technology, Chongqing, China, ³Research Institute of Exploration and Development, Liaohe Oilfield Company, Panjin, China

The complex pore structures and unclear oil-bearing controls in lacustrine shale (such as the Es4 member of the Liaohe Depression) constrain sweet spot prediction. We divided the lithofacies types of reservoirs by mineral composition and organic matter content. Combining field-scanning electron microscopy, high-pressure mercury injection, nuclear magnetic resonance, low-temperature N2 adsorption (pre- and post-oil washing), and rock pyrolysis experiments, we studied the pore structure, oil-bearing characteristics and influencing factors of shale oil reservoirs with different lithofacies. Our results identified five lithofacies in the Es4 interlayer shale, with organic-rich calcareous, felsic, and mixed shales being dominant. Among these, superior oil content in organic-rich calcareous shale is fundamentally linked to its well-developed pore network, characterized by a higher proportion of macropores and wellconnected mesopores as quantified by MIP and NMR. Inorganic mineral content primarily controls the inherent pore structure framework, while the integration of lithofacies and resultant pore geometry ultimately governs the oil-bearing of shale oil. The organic-rich calcareous, felsic, and mixed shale facies in the Es4 exhibit distinct enrichment modes: the dissolution-large pore free oil, microfracture ink-bottle pore dual mode, and multi-stage composite pores, respectively. These findings not only provide critical insights into shale oil enrichment mechanisms and sweet spot prediction in the Es4 shale but also provide a reference method for shale oil enrichment prediction in other complex lacustrine basins around the world

KEYWORDS

interbedded-type shale oil, Es4 shale, Bohai Bay Basin, pore structural, oil content of shale

Introduction

The successful commercialization of shale oil in China, with production exceeding 6 million tons in 2024, underscores its potential as a pivotal unconventional resource (Yao et al., 2024; Tong et al., 2018; Zhang Y. et al., 2024). However, like many continental lacustrine basins worldwide, the organic-rich shale formations in China exhibit profound

vertical and lateral heterogeneity, posing a fundamental challenge to predicting shale oil enrichment and identifying "sweet spots". This heterogeneity is particularly pronounced in mature exploration areas like the western sag of the Liaohe Depression, where the shift from conventional to unconventional targets is imperative yet is hindered by complex reservoir characterizations.

Shale oil enrichment is known to be controlled by a complex interplay of lithofacies, organic geochemistry, pore network architecture, and preservation conditions (Yao et al., 2024; Jin et al., 2021; Guo et al., 2023; Li et al., 2022; Chang, 2023; Wadas et al., 2023; Wang et al., 2024). In commercially exploited interlayer-type shale oil reservoirs—such as those in the Es4 member—heterogeneity in lithology, pore structure, and oil saturation is extreme (Jing et al., 2014; Lu et al., 2016; Saif et al., 2017; Li et al., 2019; Hu, et al., 2021; Wang, 2022; Liu et al., 2023; Zhang L. et al., 2024). While lithofacies are universally acknowledged as a primary control, a critical knowledge gap persists: a systematic, quantitative understanding of how specific lithofacies at the micro- and nano-scale govern pore geometry and oil-bearing differences remains elusive. The coupling mechanisms between lithofaciesdefined pore systems and oil enrichment patterns are inadequately quantified, limiting the development of predictive geological models (Chalmers et al., 2012; Didar and Akkutlu, 2013; Aguilera, 2016; Wang et al., 2016; Bal et al., 2023).

To address this gap, this study presents a multi-methodological investigation targeting the Es4 interlayer shale. First, lithofacies classification based on mineralogy and organic matter content is established. Subsequently, field scanning electron microscopy, high-pressure mercury injection, nuclear magnetic resonance, low-temperature $\rm N_2$ adsorption (pre- and post-oil washing), and rock pyrolysis is used to decouple the controls of lithofacies on pore structure from its effects on effective oil-bearing characteristics. The enrichment model of shale oil with different lithofacies interlayers in the Es4 shale was thus established. This study provides a mechanistic framework for sweet-spot prediction in the Es4 shale, with a methodology transferable to other lacustrine shale systems worldwide that offers a reproducible approach to heterogeneity for evaluating shale oil resources in non-marine basins.

Geological setting

The western sag of Liaohe is a secondary negative tectonic unit in the Liaohe Depression of the Bohai Bay basin. It is located in the northeastern corner of the basin and is distributed in a northeastern direction. It is a dustpan-like rift basin with east-fault and west-overlap, east-steep and west-slow (Figure 1a). Its tectonic evolution is controlled by multistage tectonic movement. Since the Paleogene, the basin has experienced strong sedimentary faulting of the Shahejie Formation and strike–slip transformation of the Dongying Formation (Li et al., 2013; Liu and He, 2019; Ma et al., 2022; Liu et al., 2023; Zhang L. et al., 2024). The study area is located in the Dujiatai–Shuguang area, which is located in the middle part of the western slope area of the western depression (Figure 1b), with its south side is close to the Panshan Chenjia sub-sag area. Thick Paleogene strata were deposited in the sag (Figure 1c). The Paleogene Shahejie Formation is the core of oil and gas exploration

in the western sag (Li et al., 2013; Liu and He, 2019; Ma et al., 2022). There are many kinds of lithologic reservoirs, such as shale, fine sandstone, siltstone, and dolomite, in the Es4 shale overlying the Dongying Formation and underlying the Fangshenpao Formation (Figure 1b). It is controlled by closed and saline lake basins and was formed in a strong reducing environment (Wu et al., 2021; Ma et al., 2022; Liu et al., 2023). It is the main target layer for shale oil exploration and development, and it is also the key layer of this study. Based on source-reservoir configuration, shale oil in the Es4 member is classified into three types: interlayer, shale, and mixed. The interlayer type, dominated by sand sheet interbeds and controlled by outer-front deltaic facies and gravity flow sand bodies, has a sand ratio of 10%-30% and single-layer sandstone thickness of 1-5 m. In the Dujiatai-Shuguang area, the Es4 is primarily composed of fan delta deposits with a sand ratio below 30%. Sand bodies fine in grain size and thin in thickness form delta-front underwater distributary channels to mouth bars and sheet sands. The planar distribution of interlayer shale oil is controlled by outerfront delta facies and gravity flow sand bodies (Li et al., 2013; Liu and He, 2019).

Samples and methods

Samples

We selected 15 shale samples from 7 representative wells in the Es4 member (Figure 1a) and processed them for multimethod analysis. Each sample was divided into three portions: one ground to 80 mesh for low-temperature $\rm N_2$ adsorption (pre- and post-oil washing); another crushed to below 200 mesh for rock pyrolysis, XRD, and total organic carbon (TOC) measurements; the third used to prepare 2.5 cm \times 5 cm plug samples for NMR, high-pressure mercury intrusion, and physical property tests. Additionally, 1-cm-thick sections were prepared from large samples for field emission scanning electron microscopy (FE-SEM) observation.

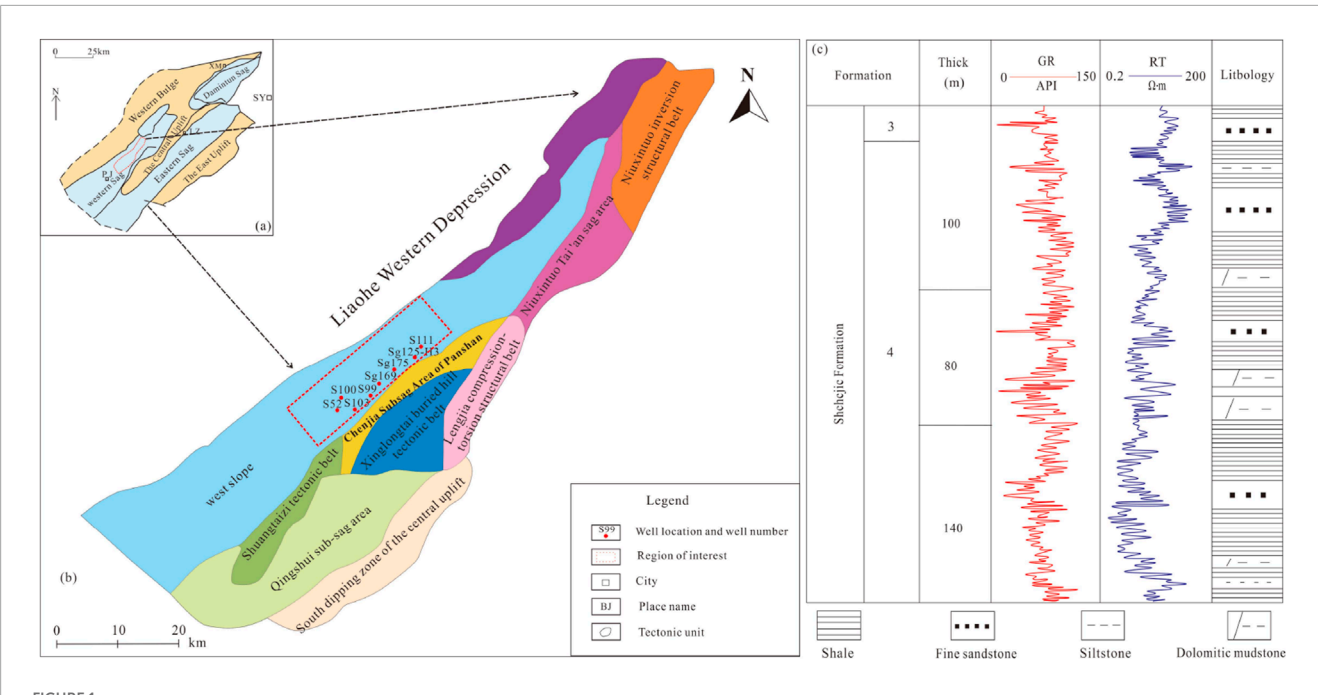
Experiments

Rock-eval pyrolysis, XRD, and TOC analysis

Powdered samples (<200 mesh) were decarbonated using 10% HCl heated in a water bath, rinsed to neutrality, and dried at 80 °C for 12 h. TOC was measured with a carbon/sulfur analyzer via combustion and standard calibration. For Rock–Eval rock pyrolysis, samples of approximately 1 g were heated from 300 °C (held 3 min) to 650 °C to quantify free hydrocarbons (S_1), pyrolysis hydrocarbons (S_2), and maximum pyrolysis peak temperature ($T_{\rm max}$). Mineral composition was determined by XRD (scan range: 5°–70°; speed: 2°/min) on pressed powder samples, with quantification using Jade 6.5 software.

FE-SEM observation

Sample blocks (1 cm \times 1 cm) were polished (sandpaper + Ar-ion milling) to create smooth surfaces (400 μ m \times 400 μ m), which were then coated with carbon and imaged with a Zeiss SU5000 FE-SEM to characterize pore systems.



Regional geological background map. (a) Division map of the tectonic area in Liaohe Depression. (b) Structural diagram of western depression and location of study area. (c) Lithological column chart of Es4.

Low-temperature N₂ adsorption

The specific surface area was measured via the BET method using an ASAP2460 analyzer on 80 mesh samples pre- and post-oil extraction.

Nuclear magnetic resonance (NMR) and high-pressure mercury intrusion (HPMI)

Low-field NMR analysis was conducted using a MesoMR23-060H-I instrument with a magnetic field strength of 0.05 \pm 0.01 T (corresponding to a proton resonance frequency of 2 MHz). Measurements were performed on both dried and oil-saturated plug samples (2.5 mm \times 5 mm) to obtain $\rm T_2$ relaxation spectra and characterize pore size distribution. HPMI utilized an AutoPore IV 9500 porosimeter with intrusion pressures up to 200 MPa to evaluate the pore and throat size distribution in dried core plugs.

Results

Organic geochemistry

Organic geochemical characterization of the Es4 shale revealed the key parameters that govern its shale oil potential (Table 1). The samples exhibited good-to-excellent hydrocarbon generation potential, with high TOC content ranging 0.46%–4.92% (avg. 3.53%), supported by high S_1 (0.07–3.46 mg/g) and S_2 (0.85–43.11 mg/g) values. Furthermore, the thermal maturity, as indicated by $T_{\rm max}$ values of 430–448 °C, places the shale within the low maturity oil window. This interpretation is corroborated by measured vitrinite reflectance ($R_{\rm o}$) values of 0.46%–0.68%. According to the correlation between HI and Tmax (Figure 2a),

the organic matter type of the Es4 shale is predominantly Types I and II_1 , with a minor proportion of Type II_2 , characteristic of a lacustrine depositional environment rich in algal organic matter. The content of vitrinite is less, the fluorescence of algae is stronger, the fluorescence of vitrinite is also weaker, and the measurement of vitrinite reflectance is further inhibited (Wenger and Baker, 1987; Wilkins et al., 1992; Josh et al., 2012; Curtis et al., 2012; Zhang Y. et al., 2024; Ma et al., 2025; Wang et al., 2025).

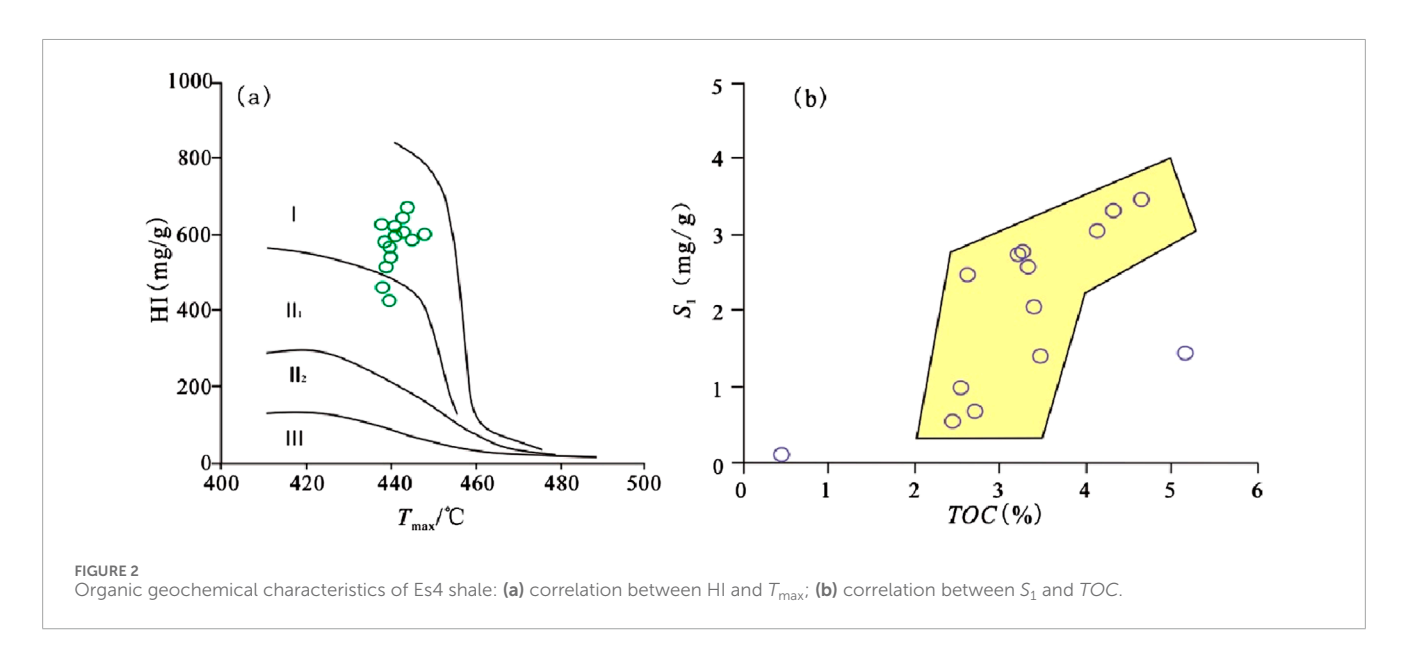
A critical insight emerges from the relationship between S_1 (free hydrocarbons) and TOC (Figure 2b). The rapid increase in S_1 within the 2% < TOC < 4% interval suggests efficient hydrocarbon generation and retention. When TOC > 4%, the growth rate gradually slows, which may indicate a threshold effect potentially related to hydrocarbon saturation or limited expulsion efficiency within the organic-rich matrix. This nonlinear relationship is a crucial control on the effective oil content in shales of varying richness.

Mineralogy and lithofacies classification

Figure 3 and Table 2 illustrate the XRD analysis results and classification scheme for the 15 shale samples. As shown in Table 2, the Es4 shale has the highest clay content, ranging 6.9%–72.7% (avg. 37.4%), followed by quartz minerals (avg. 26.6%), plagioclase (avg. 6.9%), K-feldspar (avg. 5.3%), and calcite (avg. 8.8%). Some minerals have high dolomite content of up to 81.5%. The content of other minerals is less than 5% (Figure 3a). The content of the main minerals varies greatly in different shales, reflecting the strong heterogeneity of continental shale. The ternary diagram (Figure 3b) is based on the mineral composition and TOC content of the four-element comprehensive lithofacies division

TABLE 1 TOC, lithofacies and organic geochemical parameters of shale samples.

Sample number	Depth (m)	TOC (%)	R _o (%)	S ₁ (mg/g)	S ₂ (mg/g)	T_{max}	НІ
L1	2,717.16	3.41	_	0.57	9.91	440	426.3282
L2	2,584	3.48	_	0.07	0.85	436	197.2556
L3	3,101.63	4.66	_	0.7	15.56	448	598.3881
L4	3,277.36	4.14	_	2.48	14.49	443	645.149
L5	3,276.26	3.34	_	1.46	28.79	445	585.4234
L6	3,119	3.22	0.52	1.01	16.05	444	668.1549
L7	3,091.27	3.27	0.68	0.73	43.11	438	622.975
L8	3,563.77	0.47	_	3.46	24.47	441	599.884
L9	3,563.27	2.46	_	3.05	19.17	440	536.7668
L10	3,562.67	0.46	_	1.42	16.48	439	513.9986
L11	3,561.87	4.33	_	2.06	13.61	438	460.0029
L12	3,567.87	3.88	_	2.78	16.06	439	575.9354
L13	3,566.87	4.17	_	2.74	17.12	441	617.1727
L14	3,565.87	4.92	_	2.58	17.51	443	601.7132
L15	3,564.37	3.97	0.46	3.31	21.5	440	572.5693



scheme (Li et al., 2022; Wang et al., 2024). The classification identifies three dominant lithofacies that are critical for shale oil enrichment: organic-rich mixed shale, organic-rich calcareous shale, and organic-rich felsic shale. The proportion of organic-rich and poor clay shale is small. The prevalence of these organic-rich, brittle mineral-bearing deposits suggests a favorable precondition for the development of a competent pore network capable of storing and releasing hydrocarbons.

Characteristics of different lithofacies reservoirs

Pore type

According to the FE-SEM image (Figure 4), the pore system within the low-maturity Es4 shale is dominated by inorganic pores, a direct consequence of its thermal evolution stage where organic matter (OM) has not yet generated significant internal porosity

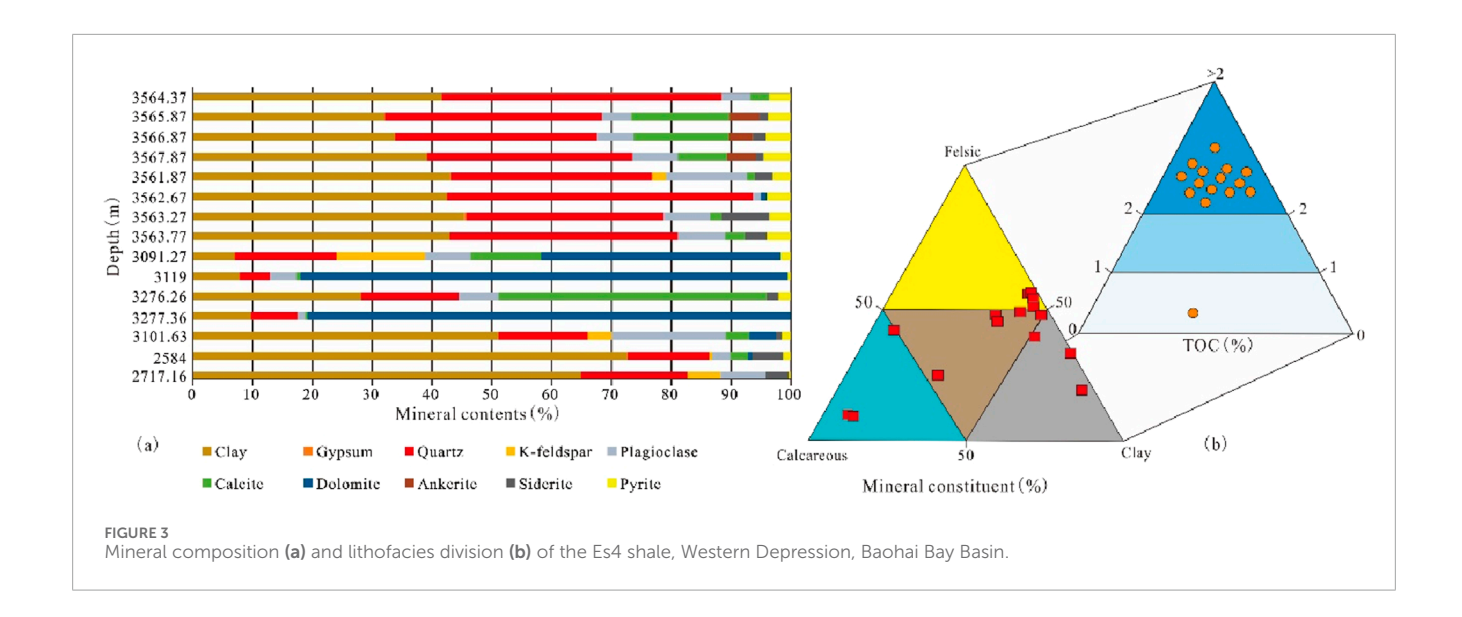


(Figure 4a). The reservoir quality is thus primarily controlled by a combination of depositional texture and diagenetic processes. There are four main types of pores: intergranular pores, intercrystalline pores, dissolution pores, and microcracks. The intergranular pores in the Es4 shale are generally developed at the edge of brittle mineral particles such as quartz and plastic organic matter or incomplete compaction between particles (Figures 4b,c), and the pores are mostly irregular multilateral shapes such as slits and wedges which can provide essential storage space and potential connectivity. Intergranular pores are mainly developed in pyrite and dolomite mineral particles, mostly irregularly shaped (Figure 4d), contributing to overall porosity but often isolated. The dissolution pores are mostly related to the interaction between organic acids and easily dissolved minerals in the hydrocarbon generation process of organic matter—mainly intergranular and intragranular dissolution. The intragranular dissolution is dominated by feldspar mineral dissolution pores and carbonate mineral dissolution pores. The pores are mostly round or oval and are often isolated (Figures 4e,f). This process significantly enhances porosity in specific lithofacies rich in these soluble minerals. In addition, the micro-cracks are mainly intergranular cracks in brittle minerals (Figure 4g), interlayer cracks in clay minerals (Figure 4h), and organic matter hydrocarbon generation shrinkage cracks (Figure 4i). They are critical for providing permeability pathways, effectively connecting otherwise isolated pore networks. In low-maturity shales such as Es4, the effective reservoir space is not the porosity provided by organic matter but the combination of primary intergranular pores and secondary dissolution pores contributing to the reservoir space. Microfractures are important transport systems.

Nitrogen adsorption hysteresis loop

Low-temperature nitrogen adsorption analysis on oil-washed samples reveals distinct pore network architectures across different lithofacies, as defined by their adsorption–desorption isotherms and hysteresis loop shapes (Figure 5). All samples exhibit Type IV isotherms with H1, H2, and H3-type hysteresis loops, indicative of complex pore systems containing cylindrical, ink-bottle, and slit-like pores, respectively (IUPAC et al., 1994). This aligns with

FE-SEM observations and provides quantitative evidence for pore geometry. The clay minerals have strong adsorption, and the adsorption capacity of rich/poor organic clay shale is large. The organic clay composite pores are developed in the organic-rich clay shale, and the pores are ink-bottle shaped (Figure 5a). The organicpoor clay shale mainly develops intergranular and interlayer pores of clay minerals—mainly slit-type pores (Figure 5b). Due to porethroat restriction, it is difficult for larger nitrogen molecules to enter larger pores through smaller pore throats in low temperature nitrogen adsorption experiments. Therefore, the adsorption amount measured by organic-rich clay shale mainly reflects adsorption near the pore throat surface, the outer surface of the particles, and a small number of pore openings, and the overall adsorption amount is lower than that of organic-poor clay shale (Figures 5a,b). The organic-rich mixed shale is controlled by multi-mineral mixing, and the pore morphology is the coexistence of slit type and ink-bottle type (Figure 5c). The organic-rich calcareous shale has cylindrical pores and mostly develops dissolution pores (Figure 5d). Organicrich felsic shale develops ink-bottle pores (Figure 5e). The felsic minerals provide a rigid framework to protect some large pores from compaction, but the pore throat is narrowed by the shrinkage of organic matter. Therefore, lithofacies determine the pore throat geometry that controls the efficiency and mobility of oil and gas reservoirs.

Pore structure

Quantitative pore structure parameters, derived from the BET (specific surface area, SSA) and BJH (pore volume, PV) methods (Loucks et al., 2012; Vafaie et al., 2015; Kelly et al., 2016; Zhang et al., 2023; Wei et al., 2025) reveal systematic variations controlled by lithofacies (Table 3). The data delineate a clear spectrum of pore characteristics. Organic-poor clay shale exhibits the highest SSA (42.214 m²/g) and a relatively large PV (0.04 cm³/g), attributable to the abundant microporosity associated with clay mineral aggregates. In stark contrast, the organic-rich calcareous shale, a principal reservoir lithofacies, possesses the lowest SSA (3.118 m²/g) but the largest average pore diameter (11.128 nm). This inverse relationship highlights a fundamental law that clay-rich facies provide extensive

TABLE 2 Mineral composition and lithofacies distribution of interlayer shale oil.

Sample number	Depth (m)	TOC (%)	Felsic content (%)	Calcareous content (%)	Clay content (%)	Lithofacies
L1	2,717.16	3.41	30.8	0	64.7	Organic-rich clay shale
L2	2,584	3.48	17.2	3.6	72.7	Organic-poor clay shale
L3	3,101.63	4.66	37.1	8.2	49.9	Organic-rich mixed shale
L4	3,277.36	4.14	9.1	81.2	9.7	Organic-rich calcareous shale
L5	3,276.26	3.34	23	44.9	28.1	Organic-rich mixed shale
L6	3,119	3.22	9.5	82.2	7.8	Organic-rich calcareous shale
L7	3,091.27	3.27	38.9	51	6.9	Organic-rich calcareous shale
L8	3,563.77	0.47	46.1	3.3	42.9	Organic-rich mixed shale
L9	3,563.27	2.46	40.8	1.9	45.4	Organic-rich mixed shale
L10	3,562.67	0.46	52.5	1	42.5	Organic-rich felsic shale
L11	3,561.87	4.33	49.5	1.4	43.1	Organic-rich mixed shale
L12	3,567.87	3.88	41.9	8.2	39.2	Organic-rich mixed shale
L13	3,566.87	4.17	39.8	15.9	33.9	Organic-rich mixed shale
L14	3,565.87	4.92	41.2	16.4	32.1	Organic-rich mixed shale
L15	3,564.37	3.97	51.6	3.2	41.6	Organic-rich felsic shale

surface area for adsorption but are dominated by small pores, whereas calcareous facies develop larger, more capacious pores conducive to storing free hydrocarbons. The organic-rich felsic and mixed shales exhibit intermediate characteristics.

High-pressure mercury injection combined with nuclear magnetic resonance is used to realize the full-aperture characterization of the interlayer shale oil of Es4 shale in the western sag of Liaohe. See the literature for data processing and the method calculation process (Chalmers et al., 2012; Daigle et al., 2014; Chen et al., 2018; Fleury et al., 2022; Liu et al., 2023). The pore size distribution shows bimodal characteristics. Organic-rich/poor clay shales show a dominant left peak (<10 nm), indicating a pore system governed by clay-related micropores and mesopores (Figures 6a,b). This structure offers high surface area for adsorption. The left peak of the organic-rich mixed shale moves slightly to the right, and the right peak becomes larger (Figure 6c). The pore size

of 0.01-100 nm contributes to the total pore volume. The pore development size is different, and the heterogeneity is strong. The left peak of the organic-rich calcareous shale continues to move to the right, and the right peak becomes larger (Figure 6d). The pore size of 1-100 nm is mainly contributed by pores, and the peak poresize distribution is consistent, indicating that pore development was relatively uniform, with mainly dissolved pores. The organic-rich felsic shale has typical bimodal characteristics. The pore size of the left peak is distributed in 0.01-1 nm (Figure 6e), mainly developing intergranular dissolution pores and intragranular dissolution pores. The peak value of the right peak is distributed in 100-1,000 nm, mainly developing organic matter and brittle mineral edge shrinkage joints. According to the contribution of pores with different pore sizes to the total pores, the Es4 shale is dominated by mesoporous development. Although mesopores (particularly < 10 nm) dominate the total pore volume, the producibility of the shale is primarily

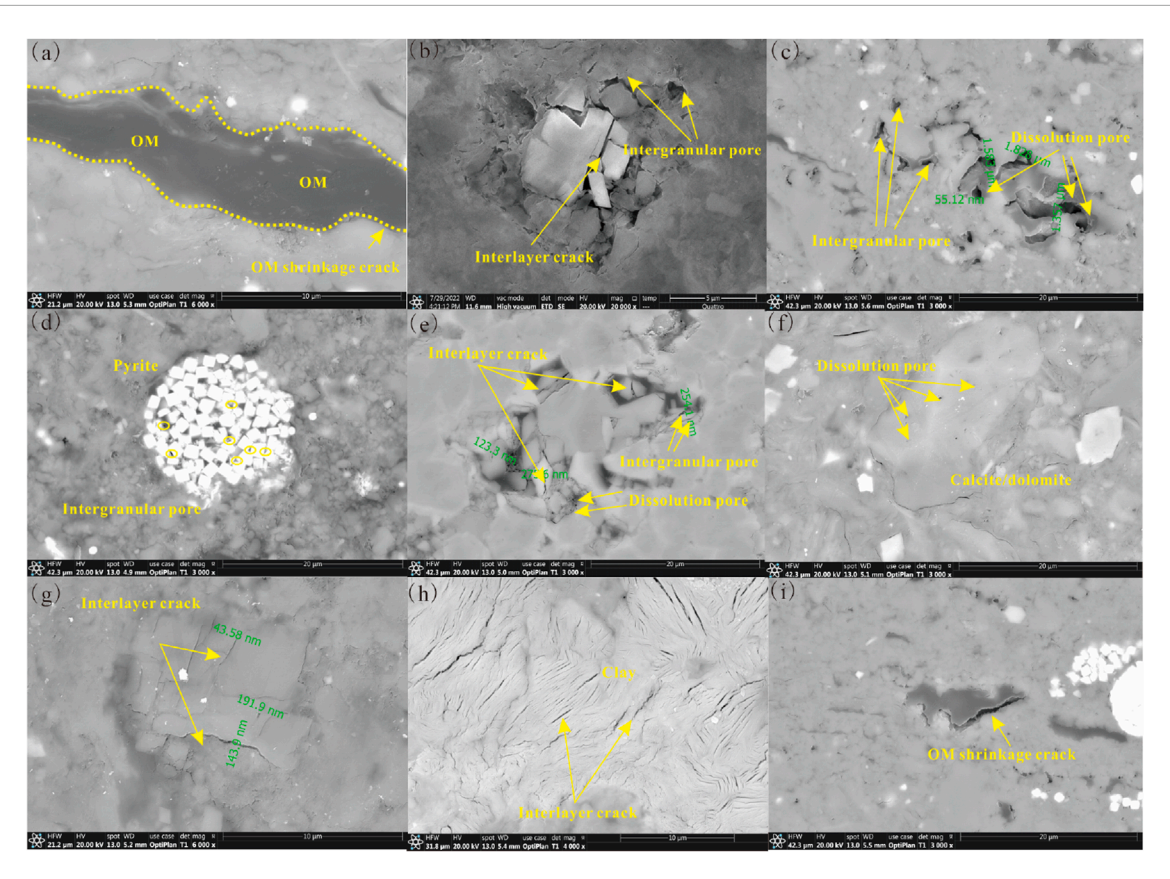


FIGURE 4
FE-SEM photos of Es4 shale pores. (a) OM pores do not develop; OM shrinkage cracks; organic-rich calcareous shale. (b) Mineral intergranular pores and mineral intergranular cracks; organic-rich felsic shale. (c) Mineral intergranular pores and dissolution pores; organic-rich felsic shale. (d) Pyrite intergranular pores; organic-rich calcareous shale. (e) Mineral intergranular pores; dissolution pores and intergranular cracks; organic-rich calcareous shale. (f) Dissolution pores; organic-rich mixed shale. (g) Intergranular cracks; organic-rich mixed shale. (h) Clay intergranular cracks; organic-poor clay shale. (i) OM shrinkage cracks; organic-rich mixed shale.

determined by the connectivity and abundance of larger mesopores and macropores (> 50 nm), which are most prevalent in calcareous and felsic lithofacies.

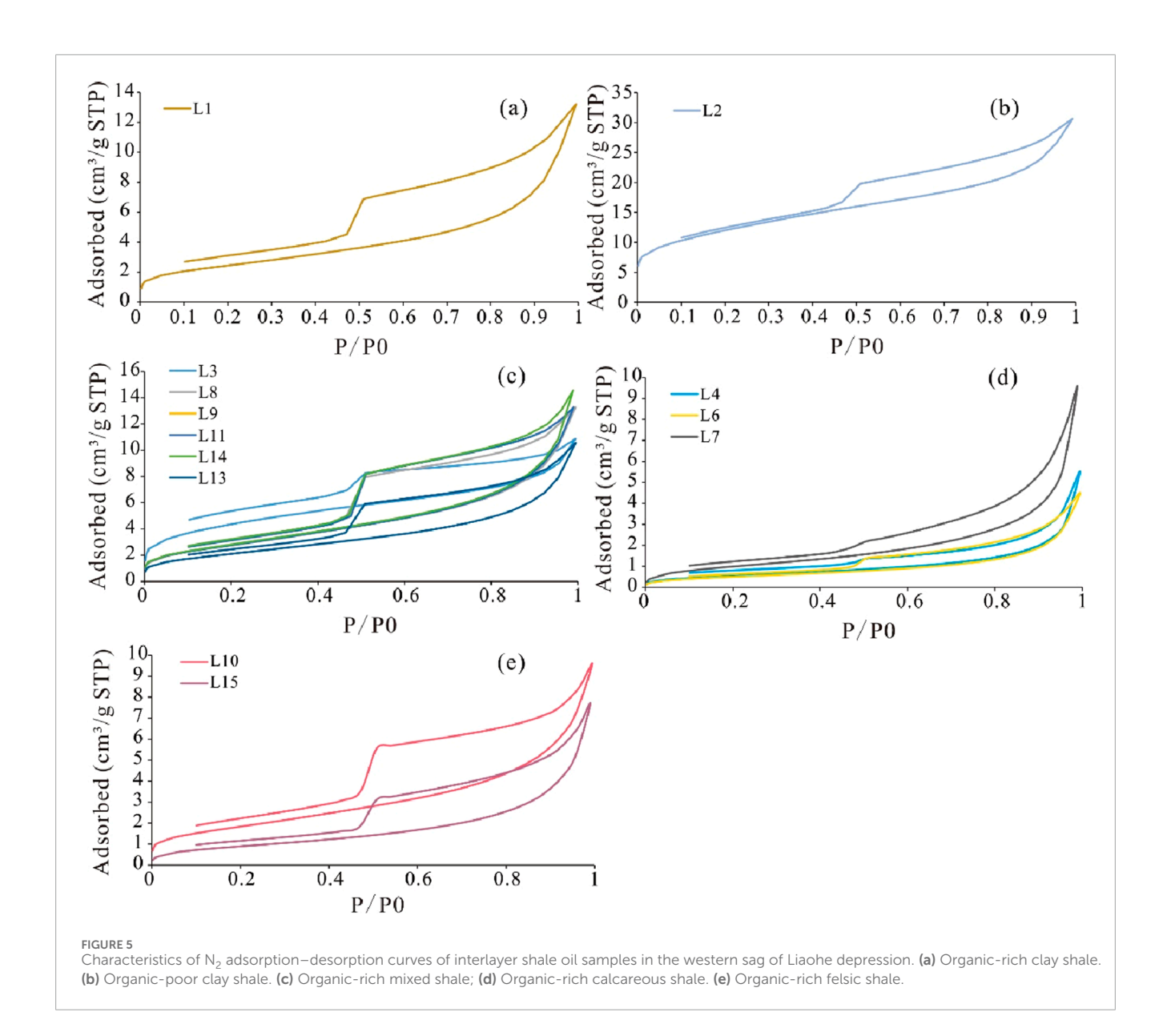
Shale oil-bearing difference

The oil-bearing properties of different lithofacies shales in Es4 shale are reflected in the occurrence characteristics, occurrence space, and oil content of hydrocarbons (Jiang et al., 2016). Core observation of typical wells in the study area revealed an obvious oil and gas taste. Some have found hydrocarbons in intergranular pores and intergranular pores such as silt particles and dolomite crystals in the interlayer shale oil reservoir of the Es4 shale through fluorescence thin-section observation; feldspar and dolomite dissolution pores and micro-cracks are filled with oil (Guo et al., 2023).

By comparing the increment of pore volume with the change of pore size measured by the nitrogen adsorption experiment of samples pre- and post-oil washing (Figure 7), the main occurrence space of residual oil in different lithofacies shale was explored. The experimental results show that the pore volume with a pore size less than 2 nm pre- and post-oil washing does not change much, indicating that pores with a size less than 2 nm are not the main storage space of residual oil.

Pore volume with a pore size of 10–100 nm changes more obviously, and pore volume with q pore size of 30–100 nm changes even more obviously, indicating that pores with a size of 30–100 nm are the main storage space of residual oil.

The pore volume of the mechanism-rich clay shale had a high value in the small pores (<10 nm) before oil washing, and the large pore section also has a certain distribution. The pore volume of the macropore section decreased slightly after oil washing (Figure 7a). The pore shape is related to the ink-bottle shape, and the pore release space is small. After oil washing, the volume of small pores and some medium pores of organic-poor clay shale becomes smaller, and the pore volume of 30–100 nm increases (Figure 7b). The pore volume of organic-rich mixed shale has a significant peak in the middle pores (approximately 10-100 nm) before oil washing. After oil washing, the pore volume increased to a certain extent from small to large pores (Figure 7c). The pore volume of organic-rich calcareous shale has a prominent peak in medium-large pores (30-100 nm and above) before oil washing. After oil washing, all pore volumes increase—related to the cylindrical pore shape—and the pores easily released during the washing process (Figure 7d). The pore volume of organic-rich felsic shale has a significant peak in the middle pores (approximately 20-100 nm) before oil washing. After oil washing, pore volumes of less than 30 nm increase, and pore volumes of more than 30 nm decrease (Figure 7e).



Therefore, the effective occurrence and mobility of shale oil are predominantly controlled by lithofacies, as it dictates pore geometry and connectivity. The dominance of meso-macropores (30–100 nm) as the primary storage space is evident, but the key insight is that the efficiency of oil release from these pores—determining its mobility—varies systematically with lithofacies due to differences in pore-throat structure (e.g., cylindrical vs. ink-bottle).

Discussion

Influencing factors of reservoir pore development

The western sag of Liaohe Depression is a deep lacustrine deposit, and the influencing factors of shale reservoir pore structure are complex, being are affected by *TOC*, mineral composition, diagenetic evolution, fluid transformation, tectonic activity, and

other factors (Chang, 2023; Liu et al., 2023; Zhang Y. et al., 2024; Zhang L. et al., 2024). There is no significant correlation between the specific surface area and pore volume of the Es4 shale and TOC distinct from typical marine shales. Because the organic matter of the continental shale reservoir is mature and low, the organic matter pores are not developed, and the contribution to the pore specific surface and pore volume is limited. In contrast, marine shale (e.g., the Longmaxi formation) has a stable mineralogy primarily composed of quartz and clay minerals, with a simpler pore system where organic matter pores contribute more significantly to porosity than in continental shales. These shales are typically more thermally mature (R_o>2.0%), promoting organic pore development. Although dissolution occurs in marine shales, it plays a subordinate role to organic-matter pores, whereas in continental shales, organic acid dissolution is key to enhancing reservoir quality (Ning et al., 2024; Miao et al., 2025).

The interlayer shale oil in the Es4 shale is dominated by inorganic pores. The PV and SSA has good correlation of shale oil in Es4,

TABLE 3 Pore structure parameters of nitrogen adsorption experiment after oil washing of different lithofacies' shale in the western sag of Liaohe.

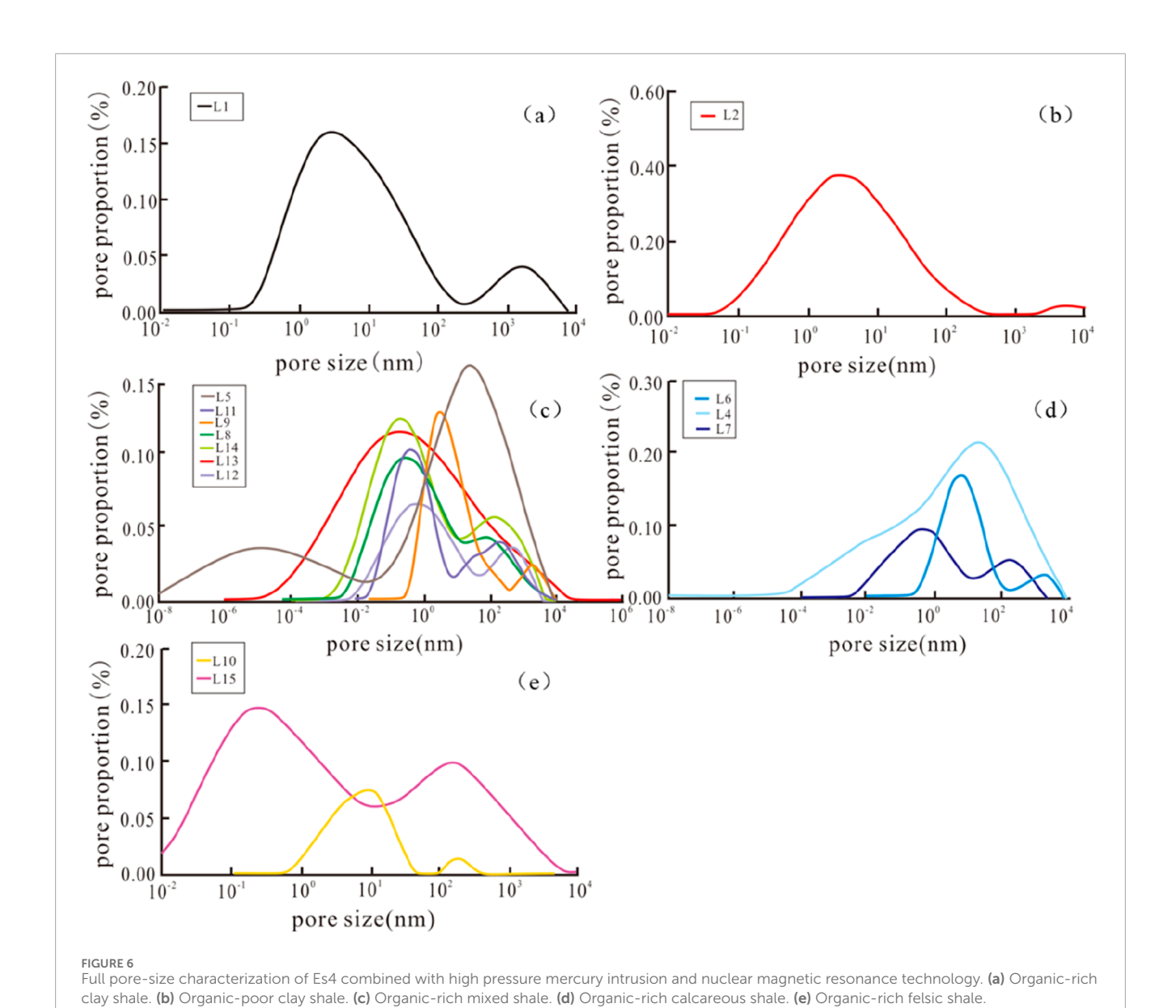
Sample number	Lithofacies	Specific surface area (m²/g)	Pore volume (cm ³ /g)	Average pore size (nm)
L1	Organic-rich clay shale	8.829	0.015	7.515
L2	Organic-poor clay shale	42.214	0.040	5.588
L3	Organic-rich mixed shale	11.197	0.015	5.209
L4	Organic-rich calcareous shale	3.680	0.010	10.500
L5	Organic-rich mixed shale	2.054	0.009	15.621
L6	Organic-rich calcareous shale	1.920	0.004	8.5273
L7	Organic-rich calcareous shale	3.753	0.0150	14.357
L8	Organic-rich mixed shale	10.293	0.020	7.863
L9	Organic-rich mixed shale	10.212	0.020	7.906
L10	Organic-rich felsic shale	6.798	0.015	8.759
L11	Organic-rich mixed shale	11.708	0.019	7.012
L12	Organic-rich mixed shale	12.130	0.022	7.353
L13	Organic-rich mixed shale	7.865	0.012	6.216
L14	Organic-rich mixed shale	10.452	0.022	8.524
L15	Organic-rich felsic shale	3.383	0.012	12.781

indicating that the developed pores are mainly small and medium and can provide both PV and SSA (Figure 8a). The pore SSA has a negative correlation with the average pore size (Figure 8b), indicating a pore network dominated by small- to medium-sized pores. This geometry provides a substantial surface area for hydrocarbon adhesion but poses challenges for fluid flow. The controlling mechanisms can be dissected by mineral type.

The strong positive correlation between SSA and clay content (Figure 8c) is mechanistically explained by the intrinsic microporosity of clay particles (e.g., illite/smectite mixed-layer). During burial diagenesis, the dehydration and illitization of smectite can generate localized micropores and microcracks. However, the ductile nature of clay minerals promotes mechanical compaction under overburden pressure, which efficiently collapses larger primary pores. This dual effect explains how weak correlation between clay content and PV (Figure 8d) clays contribute significantly to SSA (Aplin et al., 2006) but are detrimental to the preservation of the macroporosity essential for hydrocarbon storage and flow. These minerals are pivotal for creating and preserving effective pore space. The positive correlation between PV and felsic mineral content (Figure 8e) stems from their role in forming a rigid granular framework that resists compaction, thereby protecting primary intergranular pores (Dong and Harris, 2020). The negative correlation with carbonate minerals (Figure 8f) likely reflects the fact that non-dissolved, dense carbonate nodules occlude porosity, whereas dissolved carbonates are a major source of secondary porosity. Thus, the key is not just the abundance but the diagenesis of carbonate minerals. A high content of brittle minerals (especially quartz) is conducive to pore preservation and provides a material basis for later dissolution. The highest-quality reservoir occurs at an optimal balance of mineralogical components, sufficient brittle minerals to create a compaction-resistant skeleton that preserves pore volume, and a moderate clay content that contributes to storage capacity.

Influencing factors of shale reservoir oiliness

The accurate assessment of *in situ* oil content (S_1) is critical for evaluating shale oil potential, yet core storage often leads to volatile hydrocarbon loss, resulting in underestimation. The measured S_1 cannot accurately characterize the oil content in the original state of the sample (Chang, 2023; Zhang Y. et al., 2024; Zhang L. et al., 2024; Wang, 2022). Therefore, in order to realize the correction of light hydrocarbon and heavy hydrocarbon of pyrolysis parameter S_1 , it was necessary to find the S_1 recovery method in the area with similar organic geochemical characteristics (organic matter type) and similar thermal evolution degree of the fourth member of Shahejie formation in the western sag of Liaohe Depression—such as the Shahejie formation in Dongying Sag (Wang, 2022)—as shown in Formula 1. The corrected S_1 values



reveal pronounced lithofacial control: organic-rich calcareous shale exhibits the highest oil content (avg. $S_1^* = 11.367 \text{ mg/g}$), followed by mixed and felsic shales (avg. $S_1^* = 10.2 \text{ mg/g}$), with clay-rich shales enrichment occ

$$S1^* = C1 \times (S1 + S2) + S1 + C2 \times S2$$
 (1)

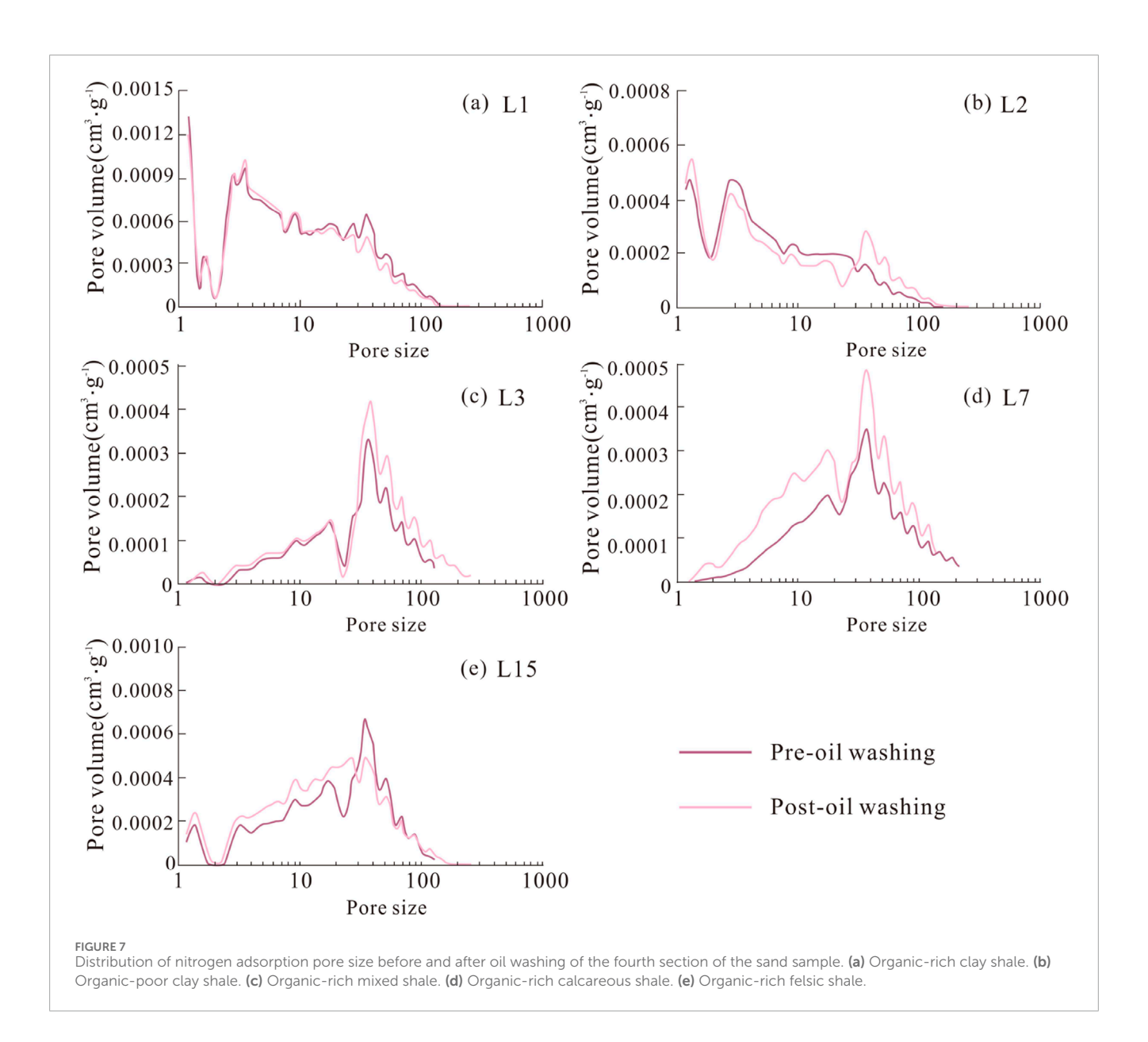
Here, S_1^* is the pyrolysis parameter of recovered light hydrocarbons, mg/g, and C1 and C2 are the light hydrocarbon and heavy hydrocarbon recovery coefficients of pyrolysis parameters—0.1 and 0.3, respectively.

showing significantly lower values.

Correlation analysis between S_1^* and TOC, $T_{\rm max}$, and hydrogen index (HI) was used after light hydrocarbon and heavy hydrocarbon correction. The strong positive correlation between S_1^* and TOC (Figure 9a) confirms the prerequisite of a sufficient hydrocarbon-generating base. Only organic matter with a certain abundance can generate shale oil and form enrichment. $T_{\rm max}$ can reflect the maturity of organic matter.

The peak in S_1^* around Tmax = 440 °C (Figure 9b) aligns with the onset of the primary oil window, indicating that optimal enrichment occurs at peak oil generation maturity. There is a positive correlation between S_1^* and HI, indicating that the better the type of organic matter, the more conducive it is to shale oil enrichment (Figure 9c).

More profoundly, the relationships with mineralogy and pore structure reveal secondary control on effective enrichment. The mineral content has a complex effect on the oil content of shale and is not affected by a single mineral. S_1^* has a positive correlation with the content of felsic minerals (Figure 9d) and has a negative correlation with the content of clay minerals (Figure 9e). With the content of carbonate rocks, it first increases and then decreases (Figure 9f). Brittle mineral-supported pore networks provide the essential volume and connectivity for storing free oil, which is more readily producible. The non-linear relationship with carbonate content (Figure 9f) suggests a threshold effect, where moderate dissolution



enhances porosity but excessive, non-dissolved carbonate acts as pore-filling cement.

In general, a certain mineral content cannot directly control the enrichment of shale oil and lithofacies, as all rock characteristics formed in a certain sedimentary environment can better reflect the enrichment of shale oil. The correlation between S_1^* and the pore structure parameters of different lithofacies shows that pore structure and physical parameters have an obvious control effect on shale oil enrichment. There is a significant negative correlation between S_1^* and specific surface area (Figure 9g). Due to the larger specific surface area, the more adsorbed oil is not conducive to shale oil enrichment. There is a positive correlation between S_1^* and pore volume (Figure 9h), indicating that the larger the pore volume, the more enriched the shale oil. No matter the smaller or larger part of the pore volume, it also has a higher S_1^* , and there is more shale oil trapped inside the pore to form enrichment. There is a good positive correlation between S_1^* and porosity (Figure 9i), indicating that the better the physical properties of shale reservoirs, the more conducive it is to the enrichment of shale oil. Therefore, shale oil enrichment is not determined by a single parameter but the result of synergy. High *TOC* and optimum maturity generate oil, and lithofacies determine the pore system as the occurrence space of free oil. This explains why organic-rich calcareous shale with both good hydrocarbon generation potential, large reservoir space, and well-connected pore structure is the best "dessert" lithofacies.

Shale oil enrichment modes of different lithofacies interlayers

The enrichment of interlayer shale oil in the western sag of Liaohe is not random but is controlled by the unique diagenesis path of lithofacies, forming different pore structures and three identifiable enrichment modes. There are three main lithofacies of interlayer shale oil in the western sag of Liaohe:

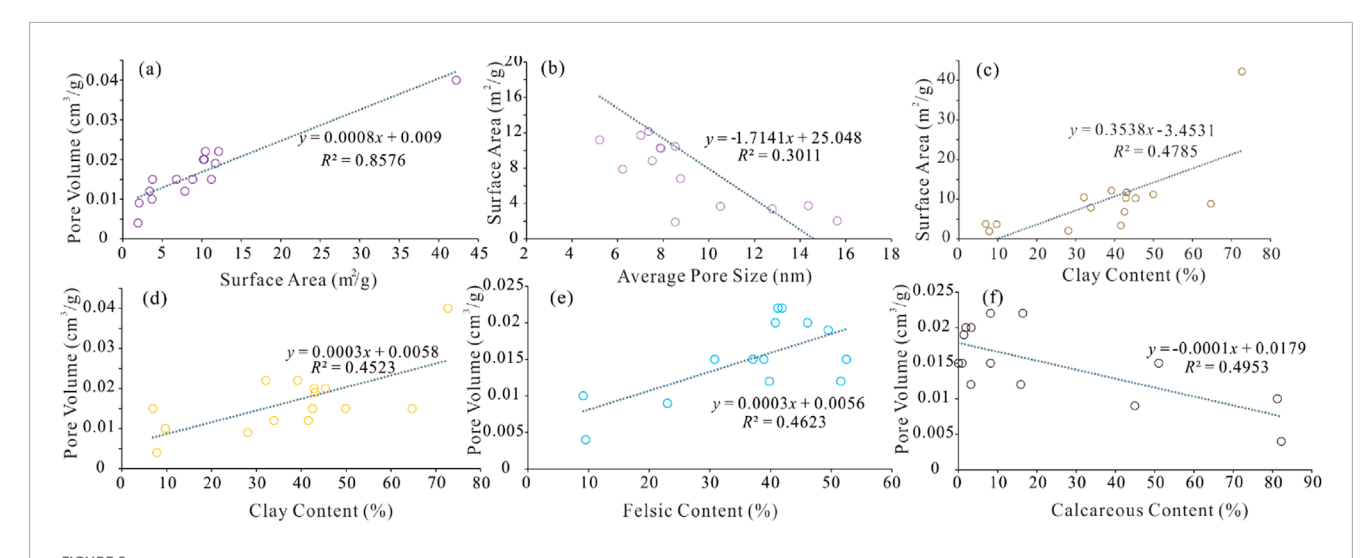
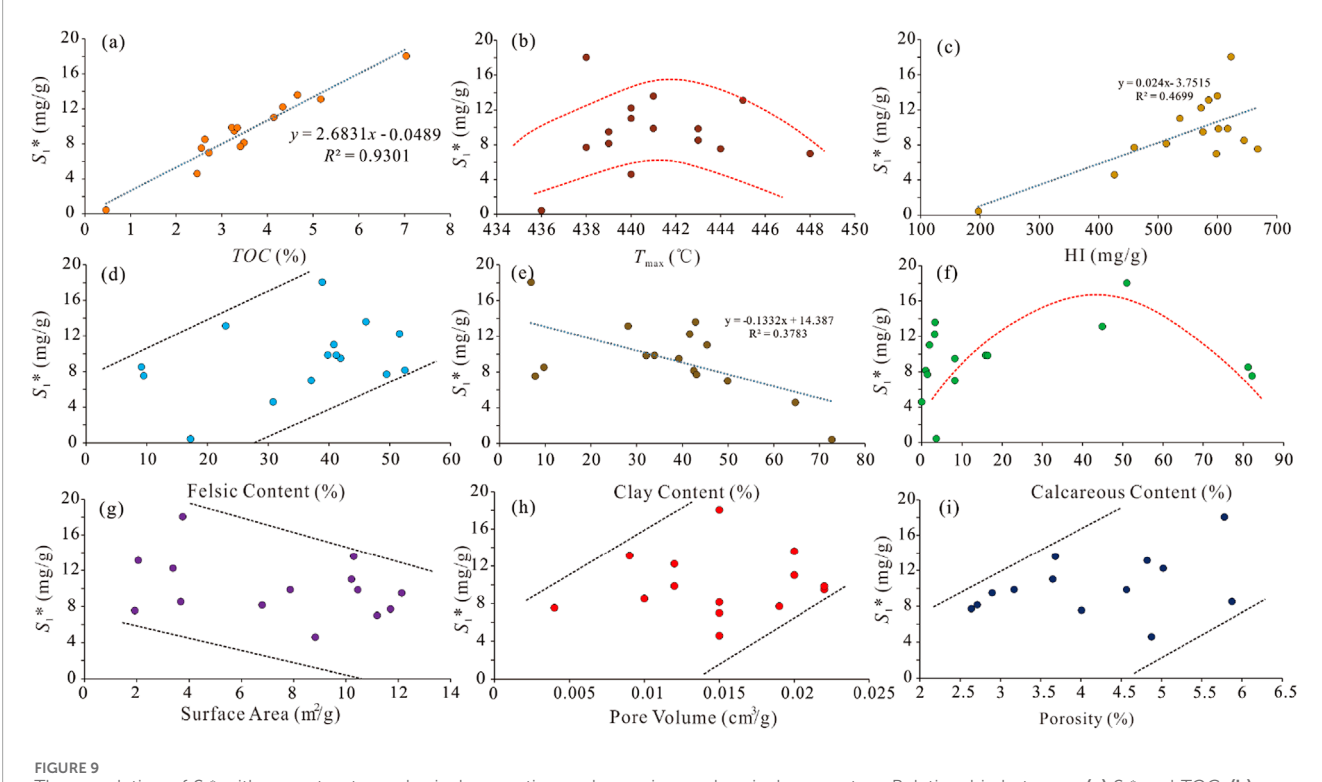


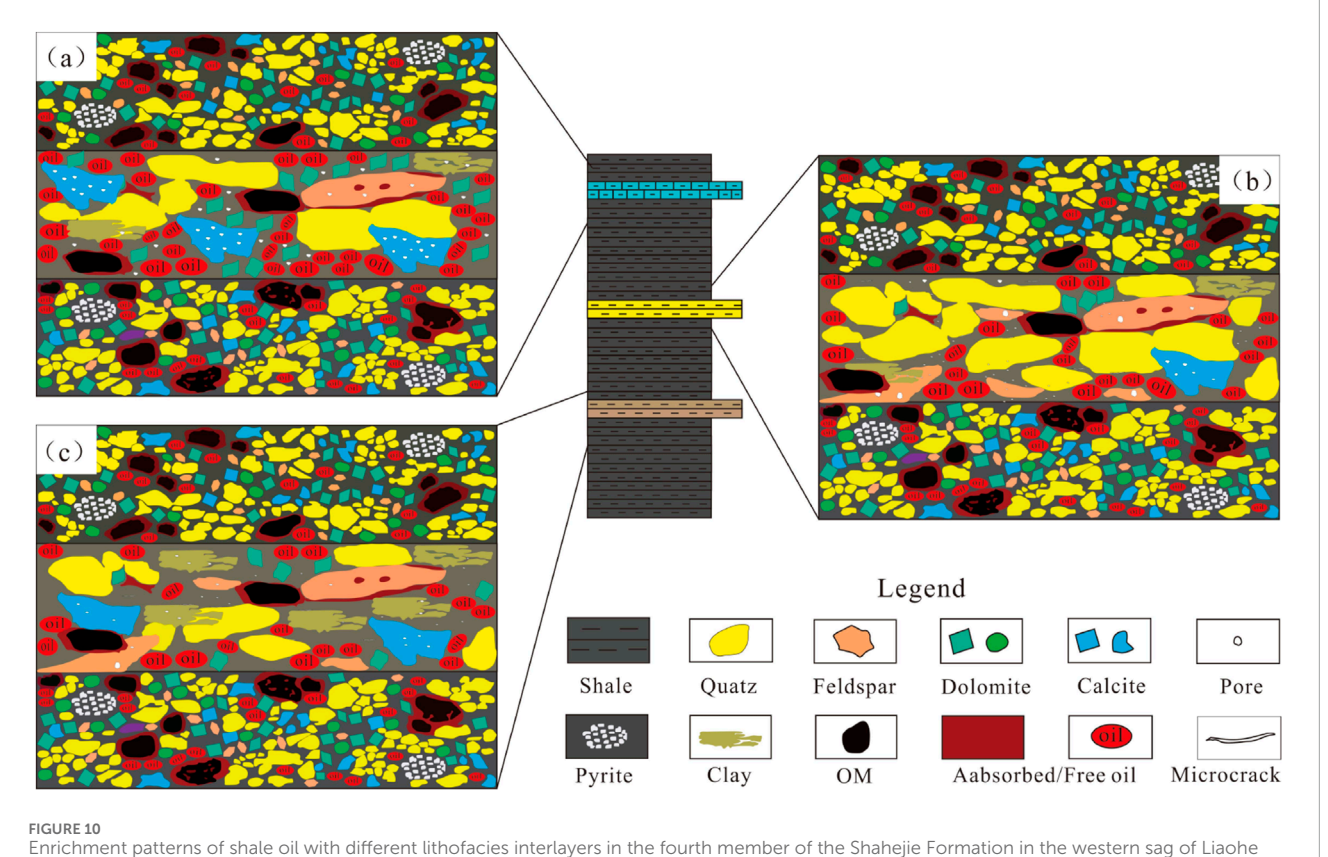
FIGURE 8
Correlation analysis of influencing factors of pore structure. Correlation between: (a) pore volume and specific surface area; (b) pore surface area and pore size; (c) pore surface area and clay mineral content; (d) pore volume and clay mineral content; (e) pore volume and felsic content; (f) pore volume and carbonate minerals.



The correlation of S_1^* with pore structure, physical properties, and organic geochemical parameters. Relationship between: (a) S_1^* and TOC; (b) S_1^* and Tmax; (c) S_1^* and HI; (d) S_1^* and felsic content; (e) S_1^* and clay content; (f) S_1^* and calcareous content; (g) S_1^* and surface area; (h) S_1^* and pore volume; (i) S_1^* and porosity.

organic-rich mixed shale, organic-rich calcareous shale, and organic-rich felsic shale. The *TOC* is high and is a high-quality source rock. Among these, the average pore size of organic-rich calcareous shale is the largest and has a good pore structure; it is a better reservoir. The occurrence state of shale oil is mainly free oil, and the oil-bearing property is the best. It

mainly occurs in 30–100 nm (Figure 5d), and the pores are mainly cylindrical (Figure 7d). The organic-rich calcareous shale has the best oil-bearing property, which is not caused by a single factor, mainly due to its superior dissolution pore connectivity and strong organic-inorganic interaction. Dissolution is the most important constructive diagenesis, contributing greatly to the pore



Depression. (a) Organic-rich calcareous shale. (b) Organic-rich felsic shale. (c) Organic-rich mixed shale.

development of shale oil reservoirs. The organic acids and CO_2 released during the maturation of organic matter (the main oil window stage) can effectively dissolve unstable minerals, mainly carbonate, and form secondary dissolution pores (intragranular dissolution pores, mold pores, and intergranular dissolution pores) and microfractures. This is one of the key mechanisms of pore development in global continental shale oil reservoirs such as the western sag of the Liaohe Depression. The interlayer shale oil of organic-rich calcareous shale facies is a dissolution pore-large pore-free oil enrichment mode (Figure 10a).

Additionally, the average pore diameter of organic-rich felsic shale is larger, and it is a dual-modal pore structure type of intergranular pore and micro-fracture. Free oil is enriched in micro-fractures, and adsorbed oil occurs in ink-bottle pores. Brittle minerals such as felsic minerals can resist compaction and protect pores during diagenesis. The organic-rich felsic shale facies intercalated shale oil is a micro-fracture ink-bottle-hole dual-mode pore enrichment model (Figure 10b).

The average pore diameter of organic-rich mixed shale is medium; the pore type is more complex, a multi-pore combination, and the oil-bearing property is medium. In the process of diagenesis, there is differential dissolution of minerals, and multiple minerals cooperate to form pores. The organic-rich mixed shale facies interlayer shale oil is a multi-stage pore-composite pore enrichment mode (Figure 10c). This hierarchy is fundamentally controlled by the diagenetic reactivity of the dominant minerals within each lithofacies.

Conclusion

Based on organic matter and mineral composition, the interlayer shale oil reservoirs in the Es4 member can be classified into five lithofacies, predominantly comprising organic-rich mixed shale, organic-rich calcareous shale, and organic-rich felsic shale. The reservoir space is dominated by intergranular pores, intercrystalline pores, dissolution pores, and microfractures within inorganic minerals. Pore geometries include cylindrical, ink-bottle, and slit-shaped types. Mesopores (pore size $<10~\rm nm)$ contribute the most to the total pore volume, while pores within the 30–100 nm range represent the primary storage space for residual oil.

Inorganic minerals play an important role in controlling the pore structure of reservoirs. Specific surface area and pore volume show a positive correlation with clay mineral content. However, the high plasticity of clay minerals facilitates compaction, which is unfavorable for the preservation of macropores. Pore volume correlates positively with felsic mineral content and negatively with carbonate mineral content. A high abundance of felsic minerals coupled with moderate carbonate content facilitates the formation of a rigid framework that resists compaction—key to preserving primary porosity.

Hydrocarbon-bearing capacity is co-controlled by lithofacies and pore structure. After correction for light and heavy hydrocarbons, the organic-rich calcareous shale facies exhibits the highest oil saturation, corresponding to a dissolution-pore-largepore-free oil enrichment model. The organic-rich felsic shale,

with moderately good oil content, follows next, characterized by a microfracture–ink-bottle-pore dual-mode enrichment model. The organic-rich mixed shale shows intermediate oil-bearing capacity, governed by a multi-scale composite pore network model. For lacustrine shales with low thermal evolution, the search for easily dissolved and brittle large lithofacies (such as calcareous shale and felsic shale) should be a priority for global exploration.

Data availability statement

The original contributions presented in the study are included in the article/supplementary material; further inquiries can be directed to the corresponding authors.

Author contributions

XH: Writing – original draft, Conceptualization, Writing – review and editing. RW: Resources, Supervision, Writing – review and editing. XZ: Validation, Methodology, Funding acquisition, Writing – review and editing. LZ: Resources, Funding acquisition, Project administration, Writing – review and editing. RG: Software, Investigation, Writing – review and editing. RL: Validation, Writing – review and editing, Formal Analysis. WL: Writing – review and editing, Software.

Funding

The author(s) declare that financial support was received for the research and/or publication of this article. This research was funded by the Chongqing Talent Plan "Contract System" Project (cstc2024ycjh-bgzxm0064), the Science and Technology

Research Project of Chongqing Education Commission (No. KJZD-K202401503) and the Chongqing Natural Science Foundation (cstc2021hcyj-msxmX0984).

Conflict of interest

Authors RG and WL were employed by Liaohe Oilfield Company.

The remaining authors declare that the research was conducted in the absence of any commercial or financial relationships that could be construed as a potential conflict of interest.

Generative AI statement

The authors declare that no Generative AI was used in the creation of this manuscript.

Any alternative text (alt text) provided alongside figures in this article has been generated by Frontiers with the support of artificial intelligence and reasonable efforts have been made to ensure accuracy, including review by the authors wherever possible. If you identify any issues, please contact us.

Publisher's note

All claims expressed in this article are solely those of the authors and do not necessarily represent those of their affiliated organizations, or those of the publisher, the editors and the reviewers. Any product that may be evaluated in this article, or claim that may be made by its manufacturer, is not guaranteed or endorsed by the publisher.

References

Aguilera, R. (2016). Shale gas reservoirs: theoretical, practical and research issues. *Petroleum Res.* 1, 10–26. doi:10.1016/S2096-2495(17)30027-3

Aplin, A. C., Matenaar, I. F., McCarty, D. K., and van der Pluijm, B. A. (2006). Influence of mechanical compaction and clay mineral diagenesis on the microfabric and pore-scale properties of deep-water Gulf of Mexico mudstones. *Clays Clay Min.* 54, 500–514. doi:10.1346/CCMN.2006.0540411

Bal, A., Misra, S., Mukherjee, M., Dutta, T. K., Sen, D., Patra, A., et al. (2023). Concurrent influence of geological parameters on the integrated nanopore structure and discretized pore families of the petroliferous cambay shale assessed through multivariate dependence measure. *Front. Earth Sci.* 11, 1157122. doi:10.3389/feart.2023.1157122

Chalmers, G. R., Bustin, R. M., and Power, I. M. (2012). Characterization of gas shale pore systems by porosimetry, pycnometry, surface area, and field emission scanning electron microscopy/transmission electron microscopy image analyses: examples from the barnett, woodford, haynesville, marcellus, and doig units. *AAPG Bull.* 96, 1099–1119. doi:10.1306/10171111052

Chang, J. (2023). Accumulation mechanism and mobility evaluation of shale oil in fengcheng formation of mahu sag. Beijing: China University of Petroleum. Doctoral dissertation.

Chen, G., Lu, S., Zhang, J., Pervukhina, M., Liu, K., Wang, M., et al. (2018). A method for determining oil-bearing pore size distribution in shales: a case study from the Damintun Sag, China. *J. Pet. Sci. Eng.* 166, 673–678. doi:10.1016/j.petrol.2018.03.082

Curtis, M. E., Cardott, B. J., Sondergeld, C. H., and Rai, C. S. (2012). The development of organic porosity in the woodford shale related to thermal maturity. In: SPE annual technical conference and exhibition; 2012 October 8–10; San Antonio, Texas, USA: OnePetro.

Daigle, H., Johnson, A., and Thomas, B. (2014). Determining fractal dimension from nuclear magnetic resonance data in rocks with internal magnetic field gradients. *Geophysics* 79, D425–D431. doi:10.1190/geo2014-0325.1

Didar, B. R., and Akkutlu, I. Y. (2013). Pore-size dependence of fluid phase behavior and properties in organic-rich shale reservoirs. In: SPE International Conference on Oilfield Chemistry; 2013 April 8–10; The Woodlands, Texas, USA: OnePetro.

Dong, T., and Harris, N. B. (2020). The effect of thermal maturity on porosity development in the upper Devonian–Lower Mississippian Woodford Shale, Permian Basin, US: insights into the role of silica nanospheres and microcrystalline quartz on porosity preservation. *Int. J. Coal Geol.* 217, 103346. doi:10.1016/j.coal.2019. 103346

Fleury, M., Gimmi, T., and Mazurek, M. (2022). Porewater content, pore structure and water mobility in clays and shales from NMR methods. *Clays Clay Minerals* 70, 417–437. doi:10.1007/s42860-022-00195-4

Guo, X., Ma, X., Li, M., Qian, M., and Hu, Z. (2023). Mechanisms for lacustrine shale oil enrichment in Chinese sedimentary basins. *Oil Gas. Geol.* 44, 1333–1349. doi:10.11743/ogg20230601

Hu, T., Pang, X., Jiang, F., Wang, Q., Liu, X., Wang, Z., et al. (2021). Movable oil content evaluation of lacustrine organic-rich shales: methods and a novel quantitative evaluation model. *Earth-Sci. Rev.* 214, 103545. doi:10.1016/j.earscirev.2021. 103545

IUPAC, Physical Chemistry Division Commission on Colloid and Surface Chemistry, Subcommittee on Characterization of Porous Solids, Everett, D. H., Haynes, J. M., Pernicone, N., et al. (1994). Recommendations for the characterization of porous solids (technical report). *Pure Appl. Chem.* 66, 1739–1758. doi:10.1351/pac199466081739

- Jiang, Q., Li, M., Qian, M., Li, Z., Li, Z., Huang, Z., et al. (2016). Quantitative characterization of shale oil in different occurrence states and its application. *Pet. Geol. Exp.* 38, 842–849. doi:10.11781/sysydz201606842
- Jin, Z., Wang, G., Liu, G., Gao, B., Liu, Q., Wang, H., et al. (2021). Research progress and key scientific issues of continental shale oil in China. *Acta Pet. Sin.* 42, 821–835. doi:10.7623/syxb202107001
- Jing, T., Zhang, J., Mao, J., Li, W., and Jiang, S. (2014). Geological controls and mechanism of shale gas and shale oil accumulations in Liaohe Western Depression, China. *Energy Explor. Exploit.* 32, 503–525. doi:10.1260/0144-5987.32.3.503
- Josh, M., Esteban, L., Delle, P. C., Sarout, J., Dewhurst, D. N., and Clennell, M. B. (2012). Laboratory characterisation of shale properties. *J. Pet. Sci. Eng.* 88, 107–124. doi:10.1016/j.petrol.2012.01.023
- Kelly, S., El-Sobky, H., Torres-Verdín, C., and Matthew, B. T. (2016). Assessing the utility of FIB-SEM images for shale digital rock physics. *Adv. Water Resour.* 95, 302–316. doi:10.1016/j.advwatres.2015.06.010
- Li, Z., Jia, D., Chen, W., Zhang, Y., Wang, M., Li, Y., et al. (2013). Structural deformation and evolution of right-lateral strike-slip tectonics of the Liaohe Western Depression during the early Cenozoic. *J. Asian Earth Sci.* 77, 1–11. doi:10.1016/j.jseaes.2013.08.002
- Li, X., Liu, X., Li, J., and Tian, Z. (2019). Comprehensive evaluation and exploration practice of lacustrine shale oil in the fourth member of shahejie formation in Damintun Sag, Liaohe Depression. China pet. *Explor.* 24, 636–648. doi:10.3969/j.issn.1672-703.2019.05.010
- Li, M., Ma, X., Jin, Z., Li, Z., Jiang, Q., Wu, S., et al. (2022). Diversity in the lithofacies assemblages of marine and lacustrine shale strata and significance for unconventional petroleum exploration in China. *Oil Gas. Geol.* 43, 1–25. doi:10.11743/ogg20220101
- Liu, Q., and He, L. (2019). Tectono-thermal modeling of the Bohai Bay Basin since the Cenozoic. *Chin. J. Geophys.* 62, 219–235. doi:10.6038/cjg2019M0637
- Liu, Y., Zhang, L., Zhang, X., He, X., Li, J., Xing, Y., et al. (2023). Pore structure and fractal characteristics of continental low maturity organic-rich shale in the Sha-4 member of the Liaohe Western Depression. *Energies* 16, 327. doi:10.3390/en16010327
- Loucks, R. G., Reed, R. M., Ruppel, S. C., and Hammes, U. (2012). Spectrum of pore types and networks in mudrocks and a descriptive classification for matrix-related mudrock pores. *AAPG Bull.* 96, 1071–1098. doi:10.1306/08171111061
- Lu, S., Chen, G., Wang, M., Li, J., Wang, X., Shan, J., et al. (2016). Evaluation of resource potential of shale oil enrichment in the fourth member of shahejie formation in Damintun Sag, Liaohe Depression. *Oil Gas. Geol.* 37, 8–14. doi:10.11743/ogg20160102
- Ma, C., Hu, C., Liu, X., Li, Y., Cui, J., Wu, Y., et al. (2022). Characterization and origin analysis of heavy oil in the Western sag of the Liaohe Basin. $ACS\ Omega\ 7,28985-28993$. doi:10.1021/acsomega.2c02668
- Ma, G., Chen, J., Yue, Z., Ma, Y., Wang, Y., Pang, H., et al. (2025). Molecular structure and hydrocarbon generation characteristics of kerogen in low-maturity shales: a case of the Paleocene shahejie formation in shuguang area, liaohe depression, Bohai Bay basin. *Oil Gas. Geol.* 46, 427–442. doi:10.11743/ogg20250207
- Miao, H., Jiang, Z., Gong, X., Li, C. M., Wang, D., and Wu, Q. (2025). The shale gas migration capacity of the qiongzhusi formation: implications for its enrichment model. *Phys. Fluids.* 37, 056603. doi:10.1063/5.0267742
- Ning, S., Xia, P., Hao, F., Tian, J., Fu, Y., and Wang, K. (2024). Pore fractal characteristics between marine and marine–continental transitional black shales: a case study of niutitang formation and longtan formation. *Fractal Fract.* 8, 288. doi:10.3390/fractalfract8050288
- Saif, T., Lin, Q., Butcher, A. R., Branko, B., and Martin, J. B. (2017). Multi-scale multi-dimensional microstructure imaging of oil shale pyrolysis using X-ray microtomography, automated ultra-high resolution SEM, MAPS mineralogy and FIB-SEM. *Appl. Energy* 202, 628–647. doi:10.1016/j.apenergy.2017.05.039

- Tong, X., Zhang, G., Wang, Z., Wen, Z., Tian, Z., Wang, H., et al. (2018). Distribution and potential of global oil and gas resources. *Pet. Explor. Dev.* 45, 779–789. doi:10.1016/S1876-3804(18)30081-8
- Vafaie, A., Habibnia, B., and Moallemi, S. A. (2015). Experimental investigation of the pore structure characteristics of the garau gas shale formation in the Lurestan Basin, Iran. *J. Nat. Gas. Sci. Eng.* 27, 432–442. doi:10.1016/j.jngse.2015.06.029
- Wadas, S. H., Krumbholz, J. F., Shipilin, V., Krumbholz, M., Tanner, D. C., and Buness, H. (2023). Advanced seismic characterization of a geothermal carbonate reservoir–insight into the structure and diagenesis of a reservoir in the German molasse basin. *Solid Earth*. 14, 871–908. doi:10.5194/se-14-871-2023
- Wang, D. (2022). Study on micro pore structure characteristics and controlling factors of shale reservoir in Lower Sha4 Member of Damintun Sag. Daqing: Northeast Petroleum University. Master's thesis.
- Wang, Y., Wang, X., Song, G., Liu, H., Zhu, D., Zhu, D., et al. (2016). Genetic connection between mud shale lithofacies and shale oil enrichment in Jiyang Depression, Bohai Bay Basin. *Pet. Explor. Dev.* 43, 759–768. doi:10.1016/S1876-3894/16/30091 Y
- Wang, X., Wang, M., Zhao, C., Yang, X., Jia, Y., Wu, R., et al. (2024). Reservoir characteristics and controlling factors of the middle–high maturity multiple lithofacies reservoirs of the Lianggaoshan formation shale strata in the northeastern Sichuan basin, China. *Mar. Pet. Geol.* 161, 106692. doi:10.1016/j.marpetgeo.2024.106692
- Wang, J., Shao, H., Zhang, Y., Jiang, Z., Gao, B., Li, L., et al. (2025). Multifractal characteristics of pore structure in the terrestrial shale reservoirs of the lianggaoshan formation in northeast Sichuan basin and its geological significance. *Front. Earth Sci.* 13, 1505090. doi:10.3389/feart.2025.1505090
- Wei, Z., Pang, Y., Yang, C., Cao, H., and Zhang, J. (2025). Pore structure monofractal and multifractal characteristics of high-mature organic-rich shale using $\rm N_2$ adsorption–desorption measurements. *Nat. Resour. Res.* 34, 459–482. doi:10.1007/s11053-024-10415-4
- Wenger, L. M., and Baker, D. R. (1987). Variations in vitrinite reflectance with organic facies—Examples from Pennsylvanian cyclothems of the midcontinent, USA. *Org. Geochem.* 11, 411–416. doi:10.1016/0146-6380(87)90075-1
- Wilkins, R. W. T., Wilmshurst, J. R., Russell, N. J., Hladky, G., Ellacott, M. V., and Buckingham, C. (1992). Fluorescence alteration and the suppression of vitrinite reflectance. *Org. Geochem.* 18, 629–640. doi:10.1016/0146-6380(92)90088-f
- Wu, Z., Zhao, X., Wang, E., Pu, X., Lash, G. G., Han, W., et al. (2021). Sedimentary environment and organic enrichment mechanisms of lacustrine shale: a case study of the Paleogene shahejie formation, Qikou sag, Bohai Bay basin. *Palaeogeogr. Palaeoclimatol. Palaeoecol.* 573, 110404. doi:10.1016/j.palaeo.2021.110404
- Yao, Y., Xiao, F., Li, S., Yang, J., Huang, Y., and Ye, C. (2024). Enrichment model of tight shale oil in the first member of Cretaceous qingshankou formation in the southern qijiasag, songliao basin. *Acta Geol. Sin.* 98 (11), 3393–3407. doi:10.19762/j.cnki.dizhixuebao.2024423
- Zhang, X., Wang, D., Zhang, L., Xing, Y., Zhang, Y., Wang, W., et al. (2023). Research on microscopic pore structure characteristics and influencing factors of shale reservoirs: a case study of the second member of the Permian lucaogou formation in Malang sag, Santanghu basin. *Energies* 16 (5), 2453. doi:10.3390/en16052453
- Zhang Y., Y., Chang, J., Jiang, Z., Gao, Z., Zhang, C., Wang, G., et al. (2024). Visualization of dynamic micro-migration of shale oil and investigation of shale oil movability by NMRI combined oil charging/water flooding experiments: a novel approach. *Mar. Pet. Geol.* 165, 106907. doi:10.1016/j.marpetgeo.2024.
- Zhang L., L., Xu, S., Jin, K., Zhang, X., Liu, Y., Chen, C., et al. (2024). Study on the influencing factors of oil bearing and mobility of shale reservoirs in the fourth member of the shahejie formation in the Liaohe Western Depression. *Energies* 17, 3931. doi:10.3390/en17163931